Accepted Manuscript

Protonation behaviour of 2-phenyl-1,3-diazaazulene derivatives

Peili Sun, Danling Rao, Pu Zhang, Yujun Qin, Zhi-Xin Guo

PII: S0040-4020(17)31335-2

DOI: 10.1016/j.tet.2017.12.051

Reference: TET 29207

To appear in: *Tetrahedron*

Received Date: 25 September 2017

Revised Date: 16 December 2017

Accepted Date: 25 December 2017

Please cite this article as: Sun P, Rao D, Zhang P, Qin Y, Guo Z-X, Protonation behaviour of 2-phenyl-1,3-diazaazulene derivatives, *Tetrahedron* (2018), doi: 10.1016/j.tet.2017.12.051.

Graphical Abstract

To create your abstract, type over the instructions in the template box below.
Fonts or abstract dimensions should not be changed or altered.

Protonation behaviour of 2-phenyl-1,3-diazaazulene derivatives

Leave this area blank for abstract info.

Peili Sun, Danling Rao, Pu Zhang*, Yujun Qin and Zhi-Xin Guo*

Department of Chemistry, Renmin University of China, Beijing 100872, P. R. China

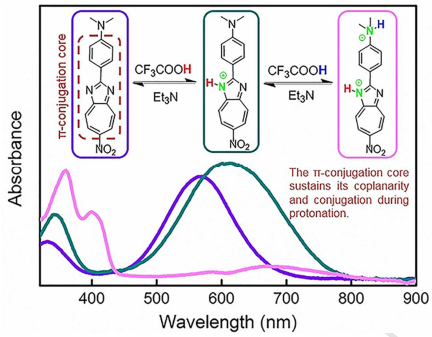

Tetrahedron
journal homepage: www.elsevier.com

Protonation behaviour of 2-phenyl-1,3-diazaazulene derivatives

Peili Sun, Danling Rao, Pu Zhang*, Yujun Qin and Zhi-Xin Guo*

Department of Chemistry, Renmin University of China, Beijing 100872, P. R. China

ARTICLE INFO

Article history:
Received
Received in revised form
Accepted
Available online

Keywords:
1,3-diazaazulene derivatives
protonation
response mechanism
π-conjugation

ABSTRACT

Three 2-phenyl-1,3-diazaazulene derivatives were synthesized and their protonation behaviours were investigated systematically *via* UV-vis absorption titration and ^{1}H NMR titration, as well as theoretical calculations. One of them exhibited a monoprotonation process while the others displayed prominent halochromic diprotonation responses. Interestingly, upon protonation of 2-phenyl-1,3-diazaazulene derivatives, the coplanarity and conjugation of the 16-π-conjugated backbones were well kept, while the electronic structures were controllably adjusted. The response mechanism of 1,3-diazaazulene derivatives towards acid is through the attachment of acid proton to the nitrogen atom in the diazaazulene ring, resulting in the change of the hybridization of protonated-N from sp^2 to sp^3, which differed from that of the well-known azulene (analogue of 1,3-diazaazulene, protonation at carbon atom). This work would provide a new insight into the protonation research of the organic functional molecules.

1. Introduction

Functional organic chromophores are drawing more and more attention due to their potential applications in optoelectronic fields,[1] including light-emitting diodes,[2] solar cells,[3,4] nonlinear optical materials,[5] and sensors.[6] The protonation of organic chromophores, which is considered as a facile and effective way to tune the transition gaps, alter the molecular interactions and control the aggregation morphology of the organic chromophores, has been one of the hottest research topics due to its potential utilities in drug delivery,[7] chemical sensors[8] and fluorescence switching devices.[9] For example, perylene bisimides were reported to exhibit near-infrared absorptions beyond 1100 nm due to the great bathochromic shift of their charge transfer bands resulted from the acid-base stimuli.[10] Dihydro-teraazaacene diimides containing 6 or 7 laterally fused six-membered rings show obvious colour changes upon protonation-deprotonation process.[11]

Generally, the response mechanism is based on the acid-base reactions between the organic chromophores and extra acid stimulus, which results in the chromophore-based cation with proton attached to a special site. Upon the transformation of the chromophore from neutral state to a positively charged cation, some properties including molecular geometry[12] and orbital energy gaps[13] could exhibit certain alterations, and some compounds even demonstrate dramatic halochromic behaviours. Usually, the molecular geometry would be greatly influenced upon protonation.

Among various organic chromophores, azulene derivatives were reported to display fine-tuned photophysical and optical behaviours owing to their unique polarized charge distribution on the fused seven- and five-membered rings,[14] thus showing great advantages as optical material candidates.[15] Researches towards azulene derivatives have also involved the halochromic responses owing to their specific structures.[16-22] It was reported that, upon protonation, the dipole moments of azulene derivatives with special substituents could be largely enhanced,[16] resulting in the adjustment of the electronic structures and the changes of corresponding physical properties, such as the typical halochromic response.[23,13,24] Studies have indicated that the protonation of azulene-based derivatives always occurs on the C1 (or C3) atom in the five-membered ring,[25,21,13,26] with the formation of tropylium cation.[27] Based on the protonation response mechanism, the protonation of azulene derivatives would undoubtedly convert the hybridization of the protonated carbon atom from sp^2 to sp^3, leading to the decrease of the molecular conjugation, which might break the planarity of azulenes and induce dramatic geometric variations.

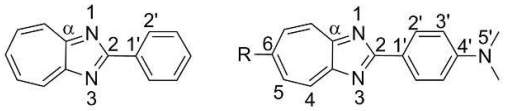

1 **2** R=H **3** R=NO_2

Scheme 1. Chemical structures for **1**, **2**, and **3**.

*Corresponding authors: Tel.: +0-106-251-2822; fax: +0-106-251-6444;
e-mail: zhangpu@ruc.edu.cn (P. Zhang), gzhixin@ruc.edu.cn (Z.X. Guo).

1,3-diazaazulene (DAA) is a unique derivative of azulene in which two carbon atoms are replaced by nitrogen atoms, with a rather large dipole moment locating within the heteroaromatic core.[28,29] Our group and collaborators have previously reported a series of donor-π-acceptor typed DAA derivatives which show relatively small ground dipole moment (μ_g) and large first-order hyperpolarizability (β).[30-32] The above mentioned DAA derivatives all contain a basic conjugated skeleton of 2-phenyl-1,3-diazaazulene (**1**, as shown in Scheme 1), which should be responsible for their superior performances in nonlinear optics. As is proved, the simple molecule **1** is coplanar, indicating that the introduction of phenyl group to 2 C atom of DAA would enlarge the conjugation system to form a 16-π-conjugated construction.[30] Meanwhile, considering the two nitrogen atoms in the five-membered ring, which would probably facilitate the protonation behaviour, it is supposed that structures based on **1** would exhibit rather novel performances compared with azulene derivatives as promising acid-stimuli responsive materials.

Thus in this paper, based on the three typical DAA derivatives 2-phenyl-1,3-diazaazulene (**1**), 2-(p-N,N-dimethylaminophenyl)-1,3-diazaazulene (**2**), and 6-nitro-2-(p-N,N-dimethylaminophenyl)-1,3-diazaazulene (**3**) (Scheme 1), the protonation behaviours were detailedly investigated through UV-vis absorption titration and ^{1}H NMR titration experiments. Moreover, the protonation mechanisms of the chromophores were proposed combined with the theoretical calculations. It was found that **1**, **2**, and **3** well kept their 16-π-conjugated and coplanar structures during protonation while the molecular HOMO-LUMO energy gaps were greatly changed, indicating that the electronic structures of the **1**-based derivatives could be well tuned *via* protonation without damaging the conjugation and planarity.

2. Results and discussion

2.1. Synthetic route

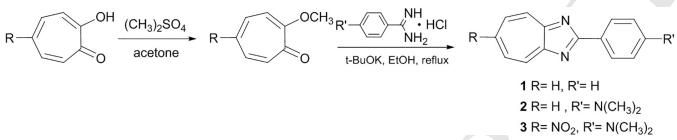

Scheme 2. Synthetic route for **1**, **2** and **3**.

Synthetic procedures for **1**, **2** and **3** were shown in Scheme 2. They were generally obtained through the condensation reactions between 2-methoxy tropone (or 2-methoxy-5-nitro tropone) and corresponding benzamidinium hydrochlorides under reflux condition, with potassium *tert*-butoxide as base and ethanol as solvent. Detailed procedures and characterizations were presented in the experimental section. **3** was synthesized according to our previous report.[33,30,32] **1** was obtained as white powder, **2** as red powder and **3** as light violet powder. They were all soluble in many organic solvents, such as dichloromethane, chloroform, ethanol, ethylacetate and so on.

2.2. UV-vis absorption studies

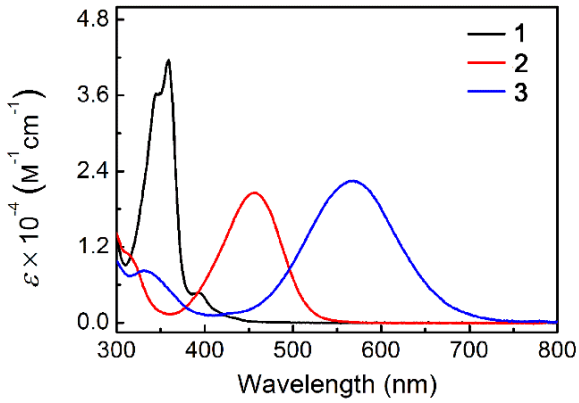

Fig. 1. UV-vis absorption spectra of **1** (20 μM), **2** (15 μM), and **3** (15 μM) in dichloromethane.

The typical UV-vis absorption spectra of **1**, **2**, and **3** measured in dichloromethane are shown in Fig. 1. **1** exhibited a major absorption band at 356 nm, similar to that of DAA.[34] Compared with **1**, a pronounced red-shift of the peak to 455 nm was observed for **2**. As for **3**, a peak with rather larger red-shift to 580 nm was obtained, with a $\Delta\lambda$ value of 224 nm compared with that of **1**. These red shifts should be caused by the introduction of electron-donating group (N,N-dimethylamino) and/or electron-withdrawing group (nitro) to **1**, which induces marked intramolecular charge transfer and tunes the electron transitions of **2** and **3**.

2.3. UV-vis absorption titration studies

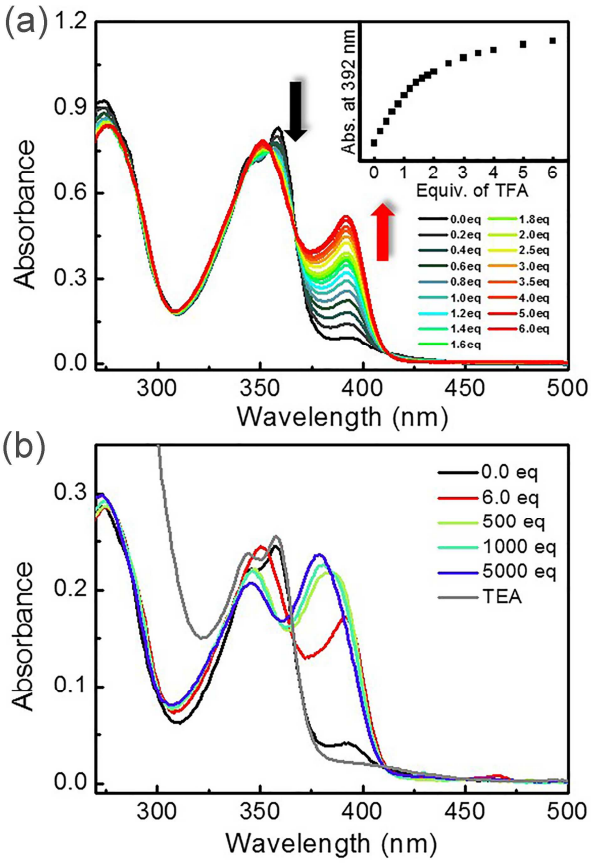

Fig. 2. UV-vis titration spectra of **1** (20 μM) upon increasing addition of TFA (a) 0.0 to 6.0 equivalents; (b) large excess equivalents, and the gray line in (b) was recorded upon the subsequent addition of TEA The inset of (a) shows: the absorption values at 392 nm *versus* equivalents of TFA.

UV-vis absorption titration, a common method for investigation of the halochromic behaviours of organic chromophores,[35,36] was used to monitor the protonation processes of **1**, **2**, and **3** in dichloromethane upon the addition of trifluoroacetic acid (TFA) as the proton donor.

With the increasing addition of TFA, the intensity of original peak of **1** at 356 nm was slowly decreased with the emerging of a new peak around 392 nm (Fig. 2a). The isobestic point at 367 nm further proved the protonation process of **1**. The absorption value at 392 nm was plotted *versus* the equivalents of TFA (inset of Fig. 2a), which exhibited a linear relationship up to 1.4 equivalent of TFA, implying that about 1.4 equivalent of TFA was needed for the one protonation of **1**. The excess addition of TFA afterwards did not induce any other new absorption peak (Fig. 2b). Subsequent addition of triethylamine (TEA) could neutralize the system back to the pristine state (the gray line in Fig. 2b). In this case, the protonation of **1** probably only need one proton, with slight solution colour change.

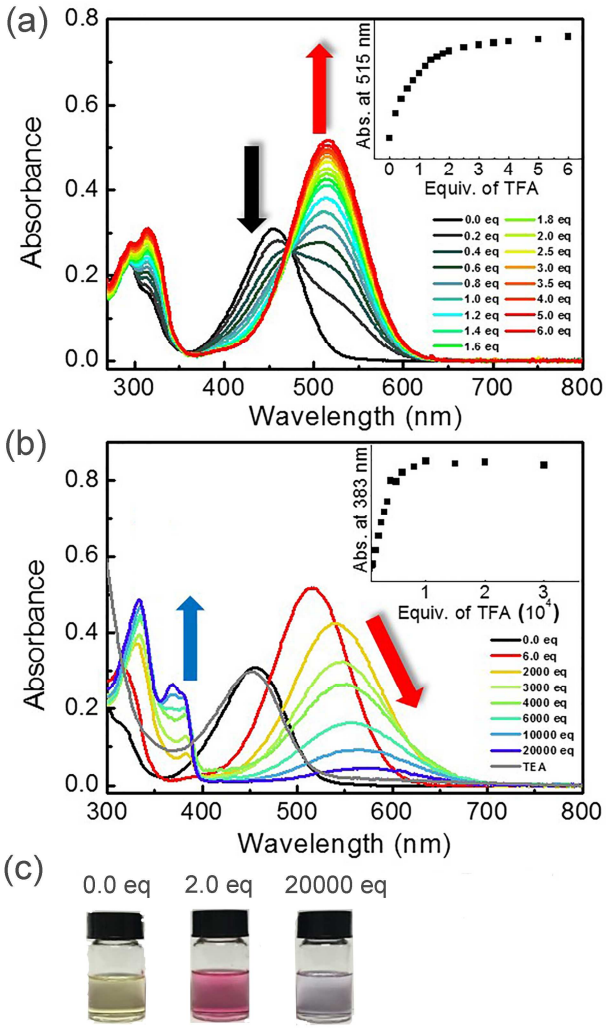

Fig. 3. UV-vis titration spectra of **2** (15 μM) upon increasing addition of TFA from (a) 0.0 to 6.0 equivalents; (b) large excess equivalents, and the gray line in (b) was recorded upon the subsequent addition of TEA; and (c) the solution colour changes of **2** under different equivalents of TFA. The insets show: (a) the absorption values at 515 nm *versus* equivalents of TFA and (b) the absorption values at 383 nm *versus* equivalents of TFA.

Fig. 3a shows the absorption spectra evolution for **2** when TFA was increased from 0 to 6 equivalents. Upon the gradual addition of TFA, a new absorption was formed at around 515 nm. The increasing of this absorption was accompanied with the

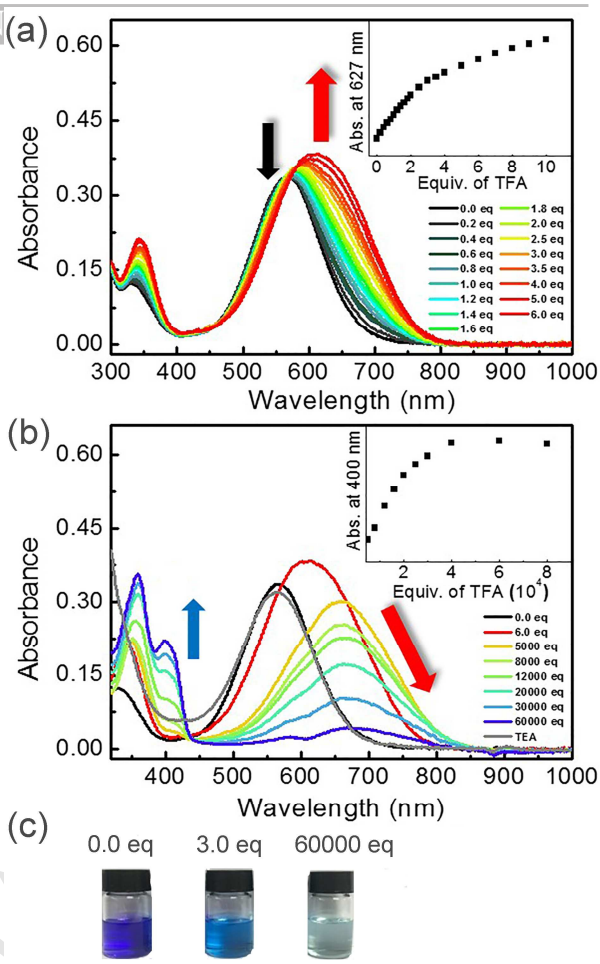

Fig. 4. UV-vis titration spectra of **3** (15 μM upon increasing addition of TFA from (a) 0.0 to 6.0 equivalents s; (b) large excess equivalents, and the gray line in (b) was recorded upon the subsequent addition of TEA; and (c) the solution colour changes of **3** under different equivalents of TFA. The insets show: (a) the absorption values at 627 nm *versus* equivalents of TFA and (b) the absorption values at 400 nm *versus* equivalents of TFA.

bleaching of the primary absorptions at 455 nm and 290 nm, respectively. The isobestic point at 477 nm indicated the spectral changes of two different species. As the equivalent of TFA was increased from 2 to 6, the peak at 515 nm was slightly red-shifted towards 520 nm, with the shape unchanged. The absorption value at 515 nm was plotted *versus* the equivalents of TFA (inset of Fig. 3a), which exhibited a linear relationship up to 1.1 equivalent of TFA, implying that about 1.1 equivalent of TFA was needed for one protonation of **2**. In addition, the solution colour gradually changed from light yellow to dark pink (Fig. 3c). However, when TFA was dramatically increased to hundreds of equivalents, another two new absorption bands near 330 nm and 380 nm arose (Fig. 3b), together with the colour changing from dark pink to colourlessness (Fig. 3c). Meanwhile, the peak at 515 nm decreased and gradually red-shifted to a more broadened band. Likewise, the isobestic point at 395 nm proved the coexistence of the initially formed species and the newly formed one. There was also a linear increase as the TFA's equivalent was increased from 1000 to 7000 (inset of Fig. 3b). Upon the continuing addition of TEA, the resulting solution also could be recovered to neutral state (the gray line shown in Fig. 3b). Thus, different from **1**, there should be a subsequent protonation of **2** which is responsive to large equivalents of acid. In this context, **2** is a double-protonated stimuli response: the first protonation is responsive to small equivalents of acid, the subsequent one is responsive to large equivalents of acid.

We also studied the UV-vis absorption properties of **2** under different addition of trifluoromethanesulfonic acid (Fig. S4). It shows that maximum absorption peaks of **2** under 1.0 and 5.0 equivalents trifluoromethanesulfonic acid are in good agreement with the results of **2** in the presence of 1.5 and thousands of equivalents of TFA, respectively.

UV-vis titration results for **3** are displayed in Fig. 4, which show similar results when compared with those of **2**. There was a new absorption at 627 nm and an isobestic point at 590 nm while the TFA was increased from 0 to 6 equivalents (Fig. 4a). The absorption value at 627 nm was plotted *versus* the equivalents of TFA (inset of Fig. 4a), which exhibited a linear relationship up to 2 equivalents of TFA, implying that about 2 equivalents of TFA was needed for one protonation of **3**. As addition of TFA was up to thousands of equivalents, the main peak around 630 nm gradually decreased and shifted towards 680 nm, together with the emerging of a new peak at 400 nm (isobestic point at 432 nm, shown in Fig. 4b). Another linear relationship from 6000 to 40000 equivalents of TFA for the absorption values at 400 nm was shown in the inset of Fig. 4b. Besides, the addition of TEA could induce the regaining of the neutral **3** (the gray line shown in Fig. 4b), indicating the reversible protonation-deprotonation processes for **3**. Different from **2**, the solution colour changed from light violet to blue and finally to colourlessness (Fig. 4c). Thus, the influence caused by protons on **3** is also a double-protonation course: the first protonation is responsive to small equivalents of acid, the subsequent one is responsive to large equivalents of acid.

2.4. ^{1}H NMR titration studies

To further confirm the results from UV-vis titration, ^{1}H NMR titration, another useful way for the research of protonation,[37,38] was also carried out to study the protonation behaviours of **1**, **2**, and **3**. For both **2** and **3**, the ^{1}H signals associated with the methyl moieties of N,N-dimethylamino phenyl groups were almost unchanged, indicating that the protons from TFA did not bind to the nitrogen atoms of the animo group, implying the binding of the protons with the nitrogen atoms in the DAA rings. Fig. 5 shows the partial ^{1}H NMR titration spectra of **1**, **2**, and **3** upon different addition of TFA from 0 to 6 equivalents. Compared with the original signals, the ^{1}H NMR spectra of the protonated ones all corresponded to symmetrical species (Fig. 5), which suggested a fast exchange of the proton binding between the two diazaazulene nitrogen atoms.[39]

As for **1**, the large shifts in the spectra were observed until the addition of 1.5 equivalents of TFA as shown in Fig. 5a. The signals of protons in the seven-membered ring exhibited similar downfield shifts, and the signals of protons in the phenyl ring showed only slight shifts. For the signal of proton H(d), an upfield shift was observed, while for the signals of H(e) and H(f), downfield shifts were observed. However, when TFA concentration was above 1.5 equivalents, the signals of the protons H(a), H(b), H(e) and H(f) displayed a slight downfield shift, and the signals of the protons H(c) behaved a slight upfield shift. Still, H(d) presented a more influenced shift than others, indicating that signal of H(d) for the protonated species was much easier to be affected by the solvent polarity. The chemical shifts of all the protons were plotted along with the equivalents of TFA (Fig. S1). The linear relationships were observed when the concentrations of TFA were from 0 to 1.5 equivalents, suggesting that about 1.5 equivalents of TFA were needed to realize the protonation of **1**, which agreed well with the UV-vis titration results.

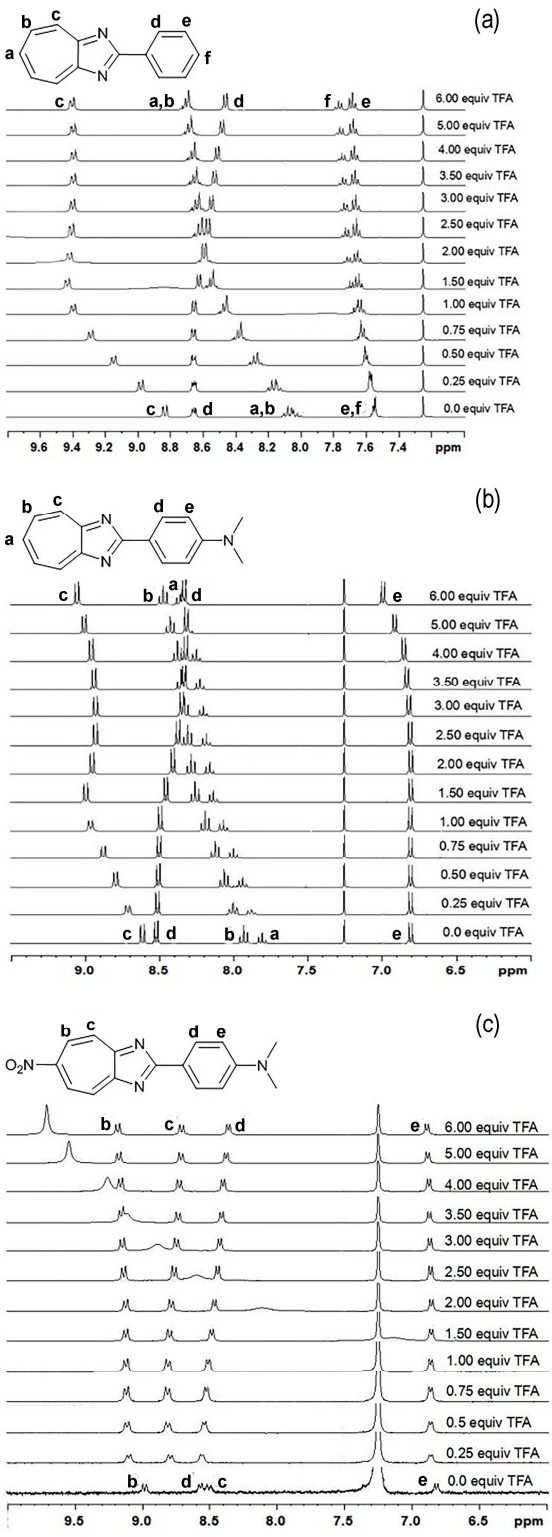

Fig. 5. Partial ^{1}H NMR titration spectra upon addition of TFA from 0 to 6 equivalents for (a) **1**, (b) **2**, and (c) **3**, respectively ($CDCl_3$ as solvent).

Equally, ^{1}H NMR protonation results of **2** are shown in Fig. 5b. Upon protonation, the signals of protons H(a) and H(b) in seven-membered ring showed similar downfield shifts, whereas that of proton H(d) exhibited an upfield shift. In addition, signal of proton H(c), which was in a smaller distance from the nitrogen atom of the conjugated ring, displayed a downfield-shift to upfield-shift behaviour, while signal of proton H(e) remained nearly unchanged. The chemical shifts of labeled protons in **2**

were plotted *versus* TFA equivalent (Fig. S2), which exhibited linear relationships under the TFA equivalent range of 0-1.2, in agreement with the first protonation course of the **2** obtained from UV-vis protonation titration results.

The ^{1}H NMR results of **2** under addition of 1.0 and 5.0 equivalents trifluoromethanesulfonic acid were also studied (Fig. 6). It can be seen that, signals of·**2** in 1.0 equivalent trifluoromethanesulfonic acid are similar to those of **2** in 1.5 equivalent trifluoroacetic acid, while signals of **2** performed downwards shifting in 5.0 equivalents trifluoromethanesulfonic acid, indicating that the second protonation should occur. The signals of protons in 5.0 equivalents trifluoromethanesulfonic acid are broad due to the poor solubility of $2H^+\cdot\mathbf{2}\cdot CF_3SO_3^-$ in chloroform.

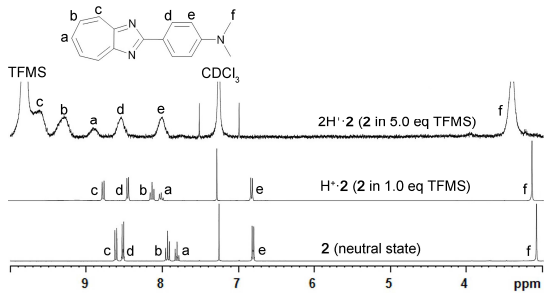

Fig. 6. Partial ^{1}H NMR results of compound **2** in neutral and protonated states. (TFMS: trifluoromethanesulfonic acid, $CDCl_3$ is used as the solvent)

For **3**, signals for each proton behaved relatively less chemical shifts compared with those of **1** and **2** (Fig. 5c). The addition of TFA initially induced downfield shifting for signals of H(b), H(c), and H(e), respectively. Later, signals for protons H(c) and H(d) exhibited an upfield shifting, while H(b) continued a downfield shifting and H(e) shifted little. The chemical shifts of labeled protons in **3** were also plotted *versus* equivalents of TFA (Fig. S3). Although there was no obvious linear relationship observed, when the equivalents of TFA were less than 2.0, the chemical shifts for each proton presented relatively regular changes, implying the completion for the first protonation of **3**, which was also in coincidence with the UV-vis titration results.

2.5. DFT studies

To further confirm the protonation sites during the protonation processes for **1**, **2**, and **3**, a theoretical study of possible protonation selection, as well as resulted protonated species, is particularly critical. In this context, DFT (density function theory) and TD-DFT (time-dependent density function theory) calculations were carried out using the Gaussian 09 software suite at the B3LYP/6-31G* level.[40]

Usually, to evaluate the protonation sites for organic compounds, proton affinity (PA), which is assumed as the negative of the enthalpy (ΔH) for the $B + H^+ \rightarrow BH^+$ process (B represents organic compound in general),[41] is essentially critical. In the meantime, the variation in zero-point vibration energies (ZPE) should be also considered. Thus, PA and ZPE were all calculated and analyzed based on the optimized geometries. Since nitrogen is demonstrated to be the most susceptible site upon proton attack in the aromatic nitrogen-containing heterocyclic compounds,[41] only the two nitrogen atoms in the five-membered ring were considered in the calculation. As the symmetry of **1** is C_{2v}, it is reasonable to only consider one nitrogen atom. While the nitrogen atom of the nitro group in **3** will not be considered for protonation, the nitrogen atom of the amino group in both **2** and **3** should not be neglected. Hence, only the PA and ZPE values of the two types of nitrogen atoms were calculated, and the results are listed in Table 1 (**2**), Table S1 (**1**), and Table S2 (**3**), respectively. **2** is representative and selected for the detailed analysis.

Table 1

The corrected zero-point vibrational energy (ZPE) and proton affinity (PA) values calculated using G09 at different sites of **2** and monoprotonated **2** ($H^+\cdot\mathbf{2}$).

Sites[a]	**2**		$H^+\cdot\mathbf{2}$	
	Scaled ZPE (au)	PA (kcal/mol)	Scaled ZPE (au)	PA (kcal/mol)
N1	0.3036	247.61	--	--
N3	0.3036	247.61	0.3166	158.64
N5'	0.3038	223.79	0.3174	161.00

[a] Sites according to Scheme 1.

For **1**, its initial protonation should only occur on one of the two nitrogen atoms. Accordingly, the subsequent protonation on the other nitrogen atom is very difficult since the PA value is rather small (Table S1). It means that only monoprotonation would occur in one of the two nitrogen atoms of **1**. This is in good accordance with the UV-vis titration as well as the ^{1}H NMR titration results.

As for **2** and **3**, the possibility of the first protonation on the amino group must be considered. However, since the PA value of the heterocyclic nitrogen atom (N1 or N3) is rather large than that of amino nitrogen atom (N5'), it's quite clear that the first protonation should occur on the one nitrogen atom of the diazaazulene ring (Table 1, Table S2). Meanwhile, since the PA value of N5' is larger than that of N3 (or N1) for the subsequent protonation, the second protonation should occur on the amino nitrogen atom (N5') for these two molecules (Table 1, Table S2).

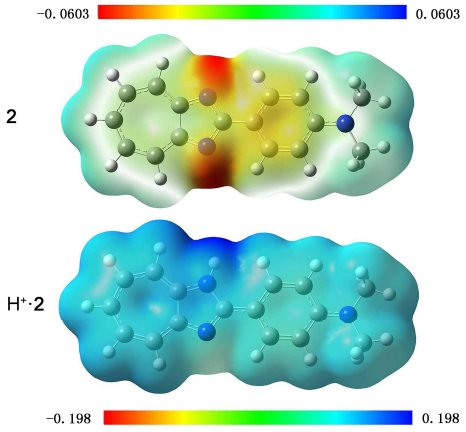

Fig. 7. ESP maps for neutral **2** and its monoprotonated species.

The above conclusion can be observed directly from the electrostatic potential (ESP) maps as well as their first protonated species (Fig. 7, Fig. S5 and Fig. S6). Clearly, each of the nitrogen atoms in the diazaazulene ring is negatively charged for the neutral **1**, **2**, and **3**, indicating that the first proton should be prioritized to bind to one of the diazaazulene nitrogen atoms. On the other hand, as can be seen from the ESP maps of the monoprotonated **1**, **2**, and **3**, since all of the three geometries are coplanar, the positive charge in the diazaazulene nitrogen atom is nearly delocalized over the whole molecule, and the positive potentials decrease along with the distance from the protonated nitrogen atom, leading to the further protonation at site N5' rather than at N3 (or N1). These results are in well accordance with Tang's report.[25]

Table 2

Summarization of HOMO, LUMO energies and corresponding maximum absorption bands of **1**, **2**, **3** and their protonated forms.

Parameters	**1**	H^+·**1**	**2**	H^+·**2**	$2H^+$·**2**	**3**	H^+·**3**	$2H^+$·**3**
E_{HOMO}[a]	-6.05	-10.03	-5.00	-8.41	-13.82	-5.40	-8.78	-13.40
E_{LUMO}[a]	-2.39	-6.69	-2.03	-6.02	-9.13	-3.05	-6.67	-9.69
ΔE[b]	3.66	3.34	2.97	2.39	4.69	2.35	2.11	3.71
λ_{max}/nm[c]	359	391	441	516	334	528	571	358
λ_{max}/nm[d]	356	390	455	515	383	590	627	400

[a] Calculated energy values using G09.
[b] $\Delta E = E_{LUMO} - E_{HOMO}$.
[c] Calculated values.
[d] Experimental values.

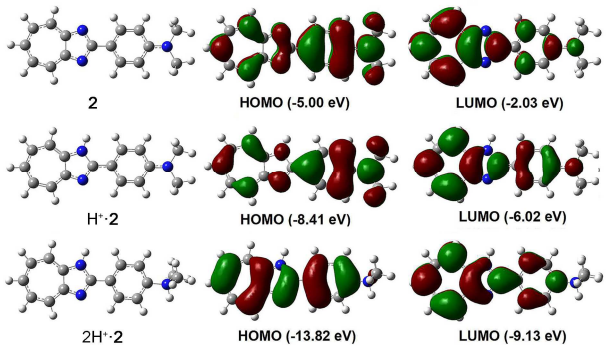

Fig. 8. Optimized geometries and molecular frontier orbitals of **2** and its protonated species.

Molecular frontier orbitals based on the optimized geometries of 1, 2, and 3 and their corresponding protonated species were calculated (Fig. 8, Fig. S7-S24, and Table S3 to Table S11). Several selected parameters are summarized in Table 2. As can be seen, both HOMO and LUMO energy levels for H+·1 (monoprotonated 1), H+·2 (monoprotonated 2) and H+·3 (monoprotonated 3) are lowered. As for H+·1, the energy gap is decreased from 3.66 eV (neutral 1) to 3.34 eV. The largest oscillator strength 0.420 of H+·1 is attributed to the transition of S0 → S2, with a maximum wavelength of 391 nm (Table S6). This agrees well with the UV-vis absorption experimental results.

In view of the optimized geometries and electronic structures of H^+·**2** and $2H^+$·**2** (diprotonated **2**), monoprotonation of **2** significantly narrows the energy gap from 2.97 eV (neutral **2**) to 2.39 eV (Table 2), corresponding to the maximum absorption wavelength of 516 nm (oscillator strength 0.4575, Table S7). This is partially resulted from the LUMO energy distribution, which is better delocalized over the whole conjugated system. However, diprotonation of **2** obviously leads to a more lowered HOMO energy level, resulting in an increased energy gap of 4.69 eV, corresponding to a maximum absorption wavelength of 334 nm (oscillator strength 0.4287, Table S8). The calculated results fit well with the UV-vis absorption experimental results, which are mainly attributed to the decreased intramolecular charge transfer as can be seen from the HOMO and LUMO charge distribution (Fig. 8).

Similarly, the calculation results of the optimized geometries and electronic structures of H^+·**3** indicate that the energy gap is narrowed from 2.35 eV (neutral **3**) to 2.11 eV (Table 2), corresponding to the maximum absorption wavelength of 571 nm (oscillator strength 0.5988, Table S9). The corresponding results of $2H^+$·**3** (diprotonated **3**, Fig. S8) show a more lowered HOMO energy level, resulting in an increased energy gap of 3.71 eV, corresponding to a maximum absorption wavelength of 358 nm (oscillator strength 0.3748, Table S10). These calculated results roughly agree with the experimental results and have the same changing tendency.

It was reported that similar to azulene and its derivatives, DAA is negatively charged in the five-membered ring.[28] Considering that the molecules investigated are conjugated, when the first protonation occurs on the nitrogen atom of the five-membered ring, the negative charge will be delocalized, and the energy gap between HOMO and LUMO will be lowered. This will lead to the red shifting of the maximum absorption peak compared with that of the corresponding neutral state. However, for **2** or **3**, the subsequent protonation takes place on the nitrogen atom of amino group, which is an electron donor in the conjugated molecule. Clearly, this binding of proton will largely reduce the electron donating effect, resulting the blue shifting of the maximum absorption of either **2** or **3** compared with that of the corresponding neutral species.

2.6. Charge distribution analysis

The NBO (natural bond orbital) value of an atom in a molecule is representative of the charge density.[42] The calculated NBO values are listed in Table 3. The NBO value of N1 (or N3) is in the order of **2** ≥ **1** > **3**. This result agrees well with the experimental results of the UV-vis and ^{1}H NMR titration, which shows the increasing need of 1.2, 1.4, and 2.0 equivalents of TFA for the first protonation of **2**, **1**, and **3**, respectively. It seems that the electron-donating group of amino in the phenyl ring can enhance the electronegativity of the five-membered ring in **2**, even though the enhancement is not strong enough to make a big difference compared with that of **1**. However, the electron-accepting group of nitro in the seven-membered ring can really reduce a great deal of the electronegativity of the five-membered ring in **3**, making it the hardest for the first protonation among the three molecules. Similarly, the NBO value of N5' of **2** is larger than that of **3**, also in good accordance with the UV-vis titration results. Again, the electron-accepting group of nitro in the seven-membered ring has big influence in reducing the electronegativity of the five-membered ring.

Table 3

The calculated NBO values of nitrogen atoms for **1**, **2**, and **3**.

Sites[a]	**1**	**2**	**3**
N1	−0.512	−0.514	−0.507
N3	−0.512	−0.514	−0.507
N5'	--	−0.430	−0.419

[a] Sites according to Scheme 1.

2.7. Molecular geometries

Table 4

Optimized geometry parameters for **2** and protonated **2**.

Molecules	Bond length (angstrom)			Angle (degree)		Dihedral (degree)
	Cα-N1	N1-C2	C2-C1'	Cα-N1-C2	N1-C2-N3	N1-C2-C1'-C2'
2	1.34	1.36	1.45	103.9	116.0	-0.09
H^+·**2**	1.37	1.39	1.43	109.2	110.1	-0.03
$2H^+$·**2**	1.37	1.38	1.47	108.4	111.5	-0.05
Δ1[a]	0.03	0.03	-0.02	5.3	-5.9	0.06
Δ2[b]	0.03	0.02	0.02	4.5	-4.5	0.04

[a] Δ1= H^+·**2** − **2**.
[b] Δ2=$2H^+$·**2** − **2**.

The selected optimized geometry parameters of **1**, **2**, **3** and their protonated derivatives are listed in Table 4 (**2**), Table S11 (**1**), and Table S12 (**3**), respectively. **2** is also selected for the explanation. For **2** and its protonated ones, the dihedral angles of N1-C2-C1'-C2' which determine the planarity of the diazaazulene ring and the phenyl ring are between 0.06 to -0.09°, indicating the diazaazulene part and the phenyl part is coplanar for either the neutral **2** or the two protonated **2**. Meanwhile, the bond lengths of Cα-N1, N1-C2, as well as C2-C1' changed less than 0.03 angstrom, and the angles of Cα-N1-C2 and N1-C2-N3 exhibited Δ values less than 5.9°. Very similar results were also obtained for those of **1** and **3** (Table S11-S12). Thus, it can be concluded that either monoprotonation or diprotonation of **1**, **2**, and **3** has little influence on their molecular skeleton geometries, indicating that the coplanar and 16-π-conjugated structure changed little during protonation. It is mainly because that during the protonation, the hybridization of the protonated diazaazulene-nitrogen atom changed from sp^2 to sp^3, inducing a smaller twist between rings and keeping its coplanarity as well as an unaffected conjugation structure.

2.8. Single crystal structure of monoprotonated 2

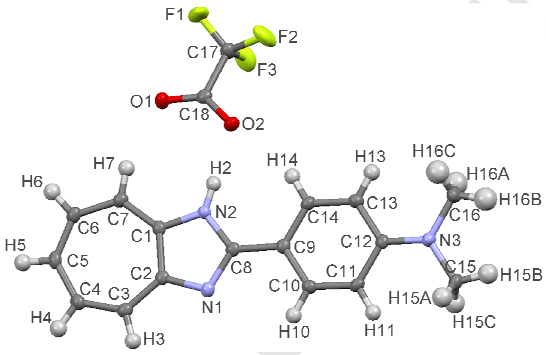

Fig. 9. Single crystal molecular structure of monoprotonated **2**.

The molecular structure of H^+·**2**·CF_3COO^- is illustrated as Oak Ridge Thermal Elliposoid Plot (ORTEP) diagram in Fig. 9. The crystal data of H^+·**2**·CF_3COO^- are listed in the supporting information (Table S13 and Table S14). Single crystal X-ray result indicates that one proton is attached to the nitrogen atom of the diazaazulene ring, forming a hydrogen bond (N2—H2···O2, with a distance of 2.683 Å). The molecular structure of H^+·**2**·CF_3COO^- shows that the diazaazulene ring and the benzene ring are almost coplanar with a dihedral angle of 1.4 (2)° (the torsion angle for N2—C8—C9—C14), implying that **2** kept its 16-π-conjugated and coplanar structure during protonation. However, although a lot of solvents have been tried, the crystals of protonated **1** and **3** were not obtained. It is possible that the changes in molecular polarity lead to a difference in crystallization.

2.9. Protonation mechanism

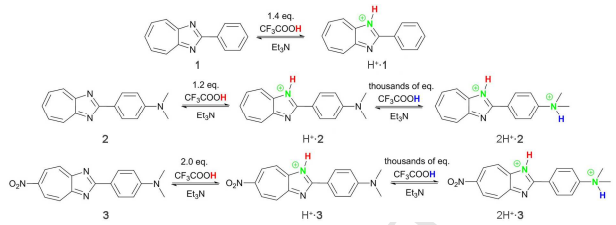

Scheme 3. Proposed protonation mechanisms of **1**, **2**, and **3**.

According to the UV-vis titration, ^{1}H NMR titration, and the theoretical calculation results, the protonation mechanisms of **1**, **2**, and **3** could be proposed as shown in Scheme 3. **1** kept its coplanar and 16-π-conjugated structure during its sole monoprotonation. **2** and **3** both went a two-step protonation with their coplanarity and 16-π-conjugated structure sustained. Hence, it could be summarized that 2-phenyl-1,3-diazaazulene is a special backbone, which is planar and π conjugated over the whole skeleton, and it could always keep its coplanarity and conjugated skeleton during protonation, different from many reported structures.[43,17]

3. Conclusion

In summary, three DAA derivatives **1**, **2**, and **3** were synthesized and their protonation behaviours and mechanisms towards TFA were investigated systematically *via* UV-vis titration, and ^{1}H NMR titration experiments, as well as theoretical calculations. As supposed, **1**, **2**, and **3** all displayed an initial nitrogen-protonation (nitrogen of the diazaazulene ring) response to the TFA stimulus, resulting in a less tendency to weaken the conjugation degree of the molecular skeleton compared with their azulene-based analogues. Besides, both **2** and **3** performed further subsequent protonation responses at the nitrogen atom of the amino group to the large amount of TFA up to thousands of equivalents. During the initial protonation process, the HOMO-LUMO energy gaps were narrowed. However, the subsequent protonation of either **2** or **3** induced great increase of HOMO-LUMO energy gaps, conducing to the bleaching of the coloured solutions. Notably, upon protonation, the molecular electronic structures of **1**, **2**, and **3** were finely tuned, while the molecular coplanarity and 16-π conjugation were sustained, which is different from many reported chromophores. Further research is undertaken for the response properties of films based on these structures, which might show promising prospects in chemical sensors and optoelectronic materials.

4. Experimental section

4.1. Materials

All reagents were purchased from *J&K* (China) and used as received unless other mentioned. Trifluoroacetic acid (99.5%) was purchased from Sigma-Aldrich. Dichloromethane (spectral grade) was purchased from *J&K* (China) for UV-vis experiments. All reagents were weighed and handled in room temperature. Flash column chromatography was performed over silica gel 200-300. All the compounds were purified by flash column chromatography and characterized by ^{1}H NMR, ^{13}C NMR, and HRMS, respectively (Please see Supporting Information).

4.2. Instrumentation

^{1}H NMR spectra were recorded on Bruker 400 or 600 MHz and the chemical shifts were reported in parts per million (δ) relative to the internal solvent signals (7.26 ppm for $CDCl_3$, and 2.50 ppm for DMSO-d_6). ^{13}C NMR spectra were obtained at Bruker 100 or 150 MHz and referenced to the internal solvent signals (central peak 77.0 ppm for $CDCl_3$). The peak patterns are indicated as follows: s, singlet; d, doublet; dd, doublet of doublet; t, triplet; q, quartet; m, multiplet. The coupling constants are reported in Hertz (Hz). APEX II (Bruker Inc.) was used for ESI-MS.

UV-vis absorption spectra were recorded on Varian Cary 50 UV-vis spectrophotometer with dichloromethane as solvent.

^{1}H NMR protonation titration spectra were recorded on Bruker 400 MHz with $CDCl_3$ as solvent.

*4.3. 2-Phenyl-1,3-diazaazulene (**1**)*

Benzamidine hydrochloride (235 mg, 1.5 mmol) was dissolved in 40 mL of anhydrous ethanol and stirred for 5 minutes. Then 2-methoxy tropone (136 mg, 1.0 mmol) was added in, followed by the addition of *t*-BuOK (168 mg, 1.5 mmol). The resulting mixture was refluxed for 3 hours. The solvent was removed, and a white solid was obtained which was subjected to flash column chromatography on silica gel with CH_3OH: CH_2Cl_2/ 1:50 as eluents. After removing of the solvent, 161 mg of white powder was obtained. Yield: 78.1%. ^{1}H NMR (600 MHz, $CDCl_3$): δ 8.82 (d, J = 10.0 Hz, 2H), 8.67-8.62 (m, 2H), 8.07 (t, J = 9.8 Hz, 2H), 8.01 (t, J = 9.7 Hz, 1H), 7.57-7.52 (m, 3H); ^{13}C NMR (150 MHz, $CDCl_3$): δ 176.84, 164.00, 137.46, 134.22, 133.08, 131.56, 129.47, 128.83, 77.21, 77.00, 76.79; HRMS (ESI): calcd for $C_{14}H_{11}N_2$, *m/z* 207.0917 [M+H$^+$]; found, *m/z* 207.0915.

*4.4. 2-(P-N,N-dimethylaminophenyl)-1,3-diazaazulene (**2**)*

4-N,N-dimethylaminno-benzamidine hydrochloride (298 mg, 1.5 mmol) was dissolved in 40 mL of anhydrous ethanol and stirred for 5 minutes. Then 2-methoxy tropone (136 mg, 1.0 mmol) was added in, followed by the addition of *t*-BuOK (168 mg, 1.5 mmol). The resulting mixture was refluxed for 3 hours. The crude product was subjected to flash column chromatography on silica gel with *n*-hexane: ethyl acetate/ 5:1 as eluents. After removing of the solvent, 174 mg of red powder was obtained. Yield: 70.0%. ^{1}H NMR (400 MHz, DMSO-d_6): δ 8.62 (d, J = 9.7 Hz, 2H), 8.38 (d, J = 8.9 Hz, 2H), 8.09 (t, J = 9.5 Hz, 2H), 8.00 (t, J = 9.8 Hz, 1H), 6.86 (d, J = 9.0 Hz, 2H), 3.06 (s, 6H); ^{13}C NMR (150 MHz, $CDCl_3$): δ 177.32, 164.40, 152.79, 135.22, 134.09, 131.64, 131.18, 120.42, 111.79, 77.28, 77.06, 76.85, 40.11; HRMS (ESI): calcd for $C_{16}H_{16}N_3$, *m/z* 250.1339 [M+H$^+$]; found, *m/z* 250.1326.

4.5. Solution preparation for UV-vis titration studies

Titration by 0 – 6 equivalents of TFA: 0, 2, 4, 6, 8, 10, 12, 14, 16, 18, 20, 25, 30, 35, 40, 50, and 60 μL of TFA (2.0 M for **1**, 1.5 M for **2** and **3**, all in dichloromethane) was added successively to 3 mL of each compound (20 M for **1**, 15 μM for **2** and **3**, all in dichloromethane) in a 1 cm × 1 cm quartz cuvette. After each addition, the solution was mixed well and then the UV-vis absorption spectrum was measured.

Titration by large equivalents, of TFA: (a) 5, 10, and 50 μL of TFA (2000 M in dichloromethane) was added successively to 3 mL of **1** (20 μM in dichloromethane) in a 1 cm × 1 cm quartz cuvette. After each addition, the solution was mixed well and then the UV-vis absorption spectrum was measured. (b) 2, 3, 4, 6, 10, and 20 μL of TFA (15000 M in dichloromethane) was added successively to 3 mL of **2** (15 μM in dichloromethane) in a 1 cm × 1 cm quartz cuvette. After each addition, the solution was mixed well and then the UV-vis absorption spectrum was measured. (c) 5, 8, 12, 20, 30, and 60 μL of TFA (15000 M in dichloromethane) was added successively to 3 mL of **3** (15 μM in dichloromethane) in a 1 cm × 1 cm quartz cuvette. After each addition, the solution was mixed well and then the UV-vis absorption spectrum was measured.

4.6. Solution preparation for ^{1}H NMR titration studies

Titration of **1** and **2**: 0, 2.5, 5.0, 7.5, 10, 15, 20, 25, 30, 40, 50, and 60 μL of TFA (5000 M in $CDCl_3$) was added successively to 600 μL of **1** or **2** (50.0 mM in $CDCl_3$) in a NMR test tube. After each addition, the solution was mixed well and then the ^{1}H NMR spectrum was measured.

Titration of **3**: 0, 2.5, 5.0, 7.5, 10, 15, 20, 25, 30, 40, 50, and 60 μL of TFA (2000 M in $CDCl_3$) was added successively to 600 μL of **3** (20.0 mM in $CDCl_3$) in a NMR test tube. After each addition, the solution was mixed well and then the ^{1}H NMR spectrum was measured.

4.7. DFT calculation

All calculations were carried out using the Gaussian 09 quantum chemistry program package.[40] DFT calculations on the geometries optimization and TD-DFT calculations on electronic structures were both performed at B3LYP/6-31G* level for the singlet ground states (gas phase). The zero-point vibrational energies (ZPE) were scaled according to Wong (0.9804).[44]

Acknowledgments

This work was supported by the Research Funds of Renmin University of China (15XNLQ04).

References and notes

1. Ostroverkhova, O. *Chem. Rev.* **2016,** *116*, 13279-13412.
2. Burroughes, J. H.; Bradley, D. D. C.; Brown, A. R.; Marks, R. N.; Mackay, K.; Friend, R. H.; Burn, P. L.; Holmes, A. B. *Nature* **1990,** *347*, 539-541.
3. Mathew, S.; Yella, A.; Gao, P.; Humphry-Baker, R.; Curchod, B. F. E.; Ashari-Astani, N.; Tavernelli, I.; Rothlisberger, U.; Nazeeruddin, M. K.; Graetzel, M. *Nat. Chem.* **2014,** *6*, 242-247.
4. Zeng, W.; Cao, Y.; Bai, Y.; Wang, Y.; Shi, Y.; Zhang, M.; Wang, F.; Pan, C.; Wang, P. *Chem. Mater.* **2010,** *22*, 1915-1925.
5. Verbiest, T.; Houbrechts, S.; Kauranen, M.; Clays, K.; Persoons, A. *J. Mater. Chem.* **1997,** *7*, 2175-2189.
6. Bansal, A. K.; Hou, S.; Kulyk, O.; Bowman, E. M.; Samuel, I. D. W. *Adv. Mater.* **2015,** *27*, 7638-7644.
7. Wang, T.; Sun, G.; Wang, M.; Zhou, B.; Fu, J. *ACS Appl. Mater. Interfaces* **2015,** *7*, 21295-21304.
8. Yao, Z.; Hu, X.; Huang, B.; Zhang, L.; Liu, L.; Zhao, Y.; Wu, H.-C. *ACS Appl. Mater. Interfaces* **2013,** *5*, 5783-5787.
9. Kwon, M. S.; Gierschner, J.; Seo, J.; Park, S. Y. *J. Mater. Chem. C* **2014,** *2*, 2552-2557.
10. Lin, M.-J.; Fimmel, B.; Radacki, K.; Wuerthner, F. *Angew. Chem. Int. Ed.* **2011,** *50*, 10847-10850.
11. Cai, K.; Yan, Q.; Zhao, D. *Chem. Sci.* **2012,** *3*, 3175-3182.
12. Zakavi, S.; Omidyan, R.; Talebzadeh, S. *RSC Adv.* **2016,** *6*, 82219-82226.
13. Zadeh, E. H. G.; Tang, S.; Woodward, A. W.; Liu, T.; Bondar, M. V.; Belfield, K. D. *J. Mater. Chem. C* **2015,** *3*, 8495-8503.
14. Kurita, Y.; Kubo, M. *J. Am. Chem. Soc.* **1957,** *79*, 5460-5463.
15. Muranaka, A.; Yonehara, M.; Uchiyama, M. *J. Am. Chem. Soc.* **2010,** *132*, 7844-7845.
16. Murai, M.; Ku, S.-Y.; Treat, N. D.; Robb, M. J.; Chabinyc, M. L.; Hawker, C. J. *Chem. Sci.* **2014,** *5*, 3753-3760.
17. Amir, E.; Murai, M.; Amir, R. J.; Cowart, J. S., Jr.; Chabinyc, M. L.; Hawker, C. J. *Chem. Sci.* **2014,** *5*, 4483-4489.
18. Tang, T.; Lin, T. T.; Wang, F. K.; He, C. B. *J. Phys. Chem. B* **2015,** *119*, 8176-8183.

19. Koch, M.; Blacque, O.; Venkatesan, K. *J. Mater. Chem. C* **2013,** *1*, 7400-7408.
20. Birzan, L.; Cristea, M.; Draghici, C. C.; Tecuceanu, V.; Maganu, M.; Hanganu, A.; Razus, A. C.; Buica, G. O.; Ungureanu, E. M. *Dyes Pigment.* **2016,** *131*, 246-255.
21. Gai, L.; Chen, J.; Zhao, Y.; Mack, J.; Lu, H.; Shen, Z. *RSC Adv.* **2016,** *6*, 32124-32129.
22. Tang, T.; Chi, H.; Lin, T. T.; Wang, F. K.; He, C. B. *Phys. Chem. Chem. Phys.* **2014,** *16*, 20221-20227.
23. Wang, F.; Lin, T. T.; He, C.; Chi, H.; Tang, T.; Lai, Y.-H. *J. Mater. Chem.* **2012,** *22*, 10448-10451.
24. Tang, T.; Lin, T. T.; Wang, F. K.; He, C. B. *Polym. Chem.* **2014,** *5*, 2980-2989.
25. Tang, T.; Lin, T.; Wang, F.; He, C. *Phys. Chem. Chem. Phys.* **2016,** *18*, 18758-18766.
26. Murai, M.; Ku, S.-Y.; Treat, N. D.; Robb, M. J.; Chabinyc, M. L.; Hawker, C. J. *Chem. Sci.* **2014,** *5*, 3753-3760.
27. Lewis, J. W.; Nauman, R. V. *Can. J. Chem.* **1985,** *63*, 2081-2085.
28. Braun, J. R.; Lin, T.-S.; Burke, F. P.; Small, G. J. *J. Chem. Phys.* **1973,** *59*, 3595-3599.
29. Nozoe, T.; Mukai, T.; Murata, I. *J. Am. Chem. Soc.* **1954,** *76*, 3352-3353.
30. Ma, X.-H.; Fu, L.-M.; Zhao, Y.; Ai, X.-C.; Zhang, J.-P.; Han, Y.; Guo, Z.-X. *J. Polym. Sci., Part B: Polym. Phys.* **2011,** *49*, 649-656.
31. Bravaya, K. B.; Grigorenko, B. L.; Nemukhin, A. V.; Zhu, Y.-J.; Zhang, J.-P. *THEOCHEM* **2008,** *855*, 40-44.
32. Zhu, Y.-J.; Qin, A.-J.; Fu, L.-M.; Ai, X.-C.; Guo, Z.-X.; Zhang, J.-P.; Ye, C. *J. Mater. Chem.* **2007,** *17*, 2101-2106.
33. Rao, D.-L.; Sun, P.-L.; Qin, Y.; Zhang, P.; Guo, Z.-X. *Mater. Lett.* **2017,** *205*, 182-185.
34. Jinguji, M.; Ashizawa, M.; Nakazawa, T.; Tobita, S.; Hikida, T.; Mori, Y. *Chem. Phys. Lett.* **1985,** *121*, 400-404.
35. Feraud, G.; Esteves-Lopez, N.; Dedonder-Lardeux, C.; Jouvet, C. *Phys. Chem. Chem. Phys.* **2015,** *17*, 25755-25760.
36. Zucchero, A. J.; Tolosa, J.; Tolbert, L. M.; Bunz, U. H. F. *Chem. Eur. J.* **2009,** *15*, 13075-13081.
37. Kim, J.; Yennawar, H. P.; Lear, B. J. *Dalton Trans.* **2013,** *42*, 15656-15662.
38. Freire, F.; Cuesta, I.; Corzana, F.; Revuelta, J.; Gonzalez, C.; Hricovini, M.; Bastida, A.; Jimenez-Barbero, J.; Asensio, J. L. *Chem. Commun.* **2007,** *43*, 174-176.
39. Dueggeli, M.; Christen, T.; von Zelewsky, A. *Chem. Eur. J.* **2005,** *11*, 185-194.
40. Frisch, M. J.; Trucks, G. W.; Schlegel, H. B.; et al. *Gaussian 09, Revision A.02*. Wallingford CT, Gaussian, Inc., 2009.
41. Russo, N.; Toscano, M.; Grand, A.; Mineva, T. *J. Phys. Chem. A* **2000,** *104*, 4017-4021.
42. Glendening, E. D.; Landis, C. R.; Weinhold, F. *Wiley. Interdiscip. Rev. Comput. Mol. Sci.* **2012,** *2*, 1-42.
43. Yamaguchi, K.; Murai, T.; Guo, J.-D.; Sasamori, T.; Tokitoh, N. *ChemistryOpen* **2016,** *5*, 434-438.
44. Wong, M. W. *Chem. Phys. Lett.* **1996,** *256*, 391-399.